J|A|C|S
ARTICLES
Published on Web 11/19/2002

Structures of Neat and Hydrated 1-Octanol from Computer Simulations

Justin L. MacCallum and D. Peter Tieleman*

Contribution from the Department of Biological Sciences, University of Calgary, 2500 University Drive NW, Calgary, AB, Canada T2N 1N4

Received June 23, 2002

Abstract: Molecular dynamics computer simulations of 1-octanol and its mixtures with water have been performed. The liquid is composed of regions enriched in either hydrocarbons or hydroxyl groups. In neat octanol, the hydroxyl groups form clusters of long, thin chains. Upon the addition of water, the clusters become longer and more spherical, forming a structure that can be described as consisting of "overlapping elongated inverse micelles". The structures of the mixtures obtained at different hydration levels are consistent with those of experimental diffraction studies of water/octanol mixtures and previous computer simulations of neat and water-satured octanol. The saturation point of the model has been calculated using the cavity-bias particle insertion method. The solubility of water in octanol is slightly too low compared to experimental results, and suggestions for possible improvements to the force field are made.

Introduction

The partitioning of small molecules in membranes and the interactions among membrane proteins and peptides and lipids is of significant interest for understanding important biomedical processes such as drug uptake and membrane protein folding and misfolding. In addition, accurate simulation models of membranes and proteins would be a useful tool in modeling membrane protein structure and studying membrane protein function. Significant progress has been made in experimental studies of membrane protein structure and folding.[1−4] Over the past few years, atomistic-level computer simulations of membrane proteins and lipids have become increasingly useful for obtaining detailed information on the interactions among lipids, proteins, and small molecules.[5−11] To obtain quantitatively accurate simulation results on the partitioning of small molecules and membrane proteins, the simulation parameters should accurately represent free energies of transfer of functional groups between water and the membrane environment. While such calculations are becoming feasible for realistic lipid models,[12−15] they are still computationally expensive, and it is worthwhile to examine simpler systems.

Neat and water-saturated octanol (1-octanol) are often used experimentally as membrane mimetics. In pharmacology, the water−octanol partition coefficient is universally used to predict the pharmocokinetic properties of drug molecules, providing a surprisingly good correlation with water−membrane partitioning.[16−19] In contrast, partitioning between water and a pure hydrocarbon yields a significantly worse correlation with drug partitioning in membranes.[17,20] In structural biology, an experimentally determined hydrophobicity scale based on the partitioning of host−guest peptides in water/octanol[21] and water/phospholipid bilayer[22] is frequently used to predict transmembrane helices. Clearly, the amphiphilic nature of octanol provides the possibility of quite different interactions with different functional groups. It apparently mimicks some of the properties of biologically relevant lipids, although it cannot form typical lipid structures such as bilayers or micelles.

The structures of octanol and its mixtures with water have proven difficult to determine. A wide variety of spectroscopic techniques have revealed clues to the structure, but most methods yield only indirect evidence. A few studies[23,24] have

* Fax: (403) 289-9311. E-mail: tieleman@ucalgary.ca.

(1) White, S. H.; Ladokhin, A. S.; Jayasinghe, S.; Hristova, K. *J. Biol. Chem.* **2001**, *276*, 32395−32398.
(2) White, S. H.; Wimley, W. C. *Annu. Rev. Biophys. Biomol. Struct.* **1999**, *28*, 319−365.
(3) Popot, J. L.; Engelman, D. M. *Annu. Rev. Biochem.* **2000**, *69*, 881−922.
(4) Popot, J. L.; Engelman, D. M. *Biochemistry* **1990**, *29*, 4031−4037.
(5) Capener, C. E.; Sansom, M. S. P. *J. Phys. Chem. B* **2002**, *106*, 4543−4551.
(6) Grossfield, A.; Woolf, T. B. *Langmuir* **2002**, *18*, 198−210.
(7) Marrink, S. J.; Tieleman, D. P. *J. Am. Chem. Soc.* **2001**, *123*, 12383−12391.
(8) Berneche, S.; Roux, B. *Nature* **2001**, *414*, 73−77.
(9) Bandyopadhyay, S.; Shelley, J. C.; Klein, M. L. *J. Phys. Chem. B* **2001**, *105*, 5979−5986.
(10) Tieleman, D. P.; Sansom, M. S. P. *Int. J. Quantum Chem.* **2001**, *83*, 166−179.
(11) Pomes, R.; Roux, B. *Biophys. J.* **2002**, *82*, 2304−2316.
(12) Xiang, T. X.; Anderson, B. D. *Biophys. J.* **2002**, *82*, 2052−2066.
(13) Jedlovszky, P.; Mezei, M. *J. Am. Chem. Soc.* **2000**, *122*, 5125−5131.
(14) Marrink, S. J.; Berendsen, H. J. C. *J. Phys. Chem.* **1996**, *100*, 16729−16738.
(15) Marrink, S. J.; Berendsen, H. J. C. *J. Phys. Chem.* **1994**, *98*, 4155−4168.
(16) Martinez, M. N.; Amidon, G. L. *J. Clin. Pharmacol.* **2002**, *42*, 620−643.
(17) Smith, R. N.; Hansch, C.; Ames, M. M. *J. Pharm. Sci.* **1975**, *64*, 599−606.
(18) Leo, A.; Hansch, C.; Elkins, D. *Chem. Rev.* **1971**, *71*, 525−616.
(19) Hansch, C.; Bjorkroth, J. P.; Leo, A. *J. Pharm. Sci.* **1987**, *76*, 663−687.
(20) Flynn, G. L. *J. Pharm. Sci.* **1971**, *60*, 345.
(21) Wimley, W. C.; Creamer, T. P.; White, S. H. *Biochemistry* **1996**, *35*, 5109−5124.
(22) Wimley, W. C.; White, S. H. *Nat. Struct. Biol.* **1996**, *3*, 842−848.
(23) Vahvaselka, K. S.; Serimaa, R.; Torkkeli, M. *J. Appl. Crystallogr.* **1995**, *28*, 189−195.
(24) Franks, N. P.; Abraham, M. H.; Lieb, W. R. *J. Pharm. Sci.* **1993**, *82*, 466−470.

used X-ray diffraction, which yields direct structural information. However, a model must be created on the basis of the diffraction data, a task that can be particularly difficult in liquid systems. Previous computer simulations[25,26] have also provided a great deal of insight into the behavior of octanol. Debolt and Kollman studied in great detail the physical properties of octanol and water-saturated octanol in simulations of 250 octanol molecules over the course of 1 ns of data gathering, at different temperatures. They also estimated the difference in partition coefficients between water and octanol for benzene and phenol.[25] In a second simulation study, Best et al. calculated partition coefficients for small organic molecules between water-saturated octanol and water and compared these with partition coefficients based on a continuum solvation model.[26]

In this paper, we examine the structures of water/octanol mixtures using extended molecular dynamics simulations and free energy calculations. A major increase in computer power since the paper of Debolt and Kollman now makes it possible to compare directly to diffraction data at different levels of hydration, varying from neat to saturated. In addition, we calculate the predicted saturation concentration of water in octanol to test the accuracy of the representation of water/octanol interactions in our simulations and suggest some ways to improve the parametrization. The resulting model of water-saturated octanol can be used to interpret experimental diffraction and spectroscopic data and will be used in further studies aimed at improving the accuracy of simulations of small molecules and proteins in membranes.

Methods

All simulations were carried out using the GROMACS 3.0[27,28] software package. In all simulations, a leapfrog[29] integrator was used with a time step of 0.02 ps. All bond lengths were constrained to their equilibrium values, using the SETTLE algorithm[30] for water and the LINCS algorithm[31] for all other bonds. A twin-range cutoff was used for the Lennard−Jones interactions, with interactions within 0.9 nm evaluated every step and interactions between 0.9 and 1.4 nm evaluated every five steps. The electrostatic interactions were evaluated using the Particle Mesh Ewald[32,33] method with tin-foil boundary conditions. The real-space interactions were evaluated using a 0.9-nm cutoff, and the reciprocal-space interactions were evaluated on a 0.12-nm grid with fourth-order spline interpolation. In all simulations, the temperature and pressure were controlled by weak coupling[34] to an external bath. The reference temperature was 298 K with a coupling constant of 0.1 ps. The box lengths were scaled isotropically to maintain a reference pressure of 1 bar using a coupling constant of 2 ps.

Two sets of simulations were carried out. The first was a set of simulations of neat octanol in the liquid and gas phases under several different force fields. The force fields used were G43a2,[35] G45a3,[36] G45a3MOD, and OPLS all atom.[37] The G45a3MOD parameters were obtained using the G45a3 Lennard−Jones parameters and scaling the OPLS-UA[38−40] charges until the heat of evaporation was correct (see Results). For the liquid phase, a starting structure was built by filling a cubic box with 512 octanol molecules and energy minimizing. This structure was equilibrated for 2 ns, after which the box volume and total potential energy had converged. A production run of 2 ns was carried out with each of the GROMOS96-based force fields using this starting structure. A similar procedure was used for the OPLS all atom model. For the gas-phase simulations, a system composed of a single octanol molecule in a $10 \times 10 \times 10$ nm^3 box was used. A long-range cutoff of 2.0 nm was used for both the electrostatic and Lennard−Jones interactions. This combination of large box size and cutoff mimics the gas phase. A leapfrog stochastic integrator[41] with an inverse friction coefficient of 0.1 ps^{-1} was used in order to prevent the kinetic energy from accumulating in overall translation and rotation of the molecule.[42] The density was obtained directly from the liquid simulation, and the heat of evaporation was obtained from

$$\Delta H_{vap} = E_{\mathrm{gas}}^{\mathrm{intra}} + E_{\mathrm{gas}}^{\mathrm{inter}} - (E_{\mathrm{liquid}}^{\mathrm{intra}} + E_{\mathrm{liquid}}^{\mathrm{inter}}) + RT \qquad (1)$$

where $E_{\mathrm{gas}}^{\mathrm{inter}}$ is assumed to be negligible.

The second set of simulations consisted of neat octanol and several different (0.1278, 0.1648, 0.2025, 0.2590, and 0.2849) mole fractions of water using G45a3MOD for the octanol parameters and the SPC[43] water model. The results presented here focus on the simulations of neat, partially hydrated (0.1648), and fully hydrated (0.2590) octanol. Analysis of the other simulations shows similar trends, with values lying between the presented ones. The systems were constructed by overlaying a preequilibrated box of water on the structure from the end of the 2 ns simulation from above. Any water molecules that overlapped with atoms from the octanol system were deleted. For each system, enough water molecules were removed to yield the correct mole fraction. The systems were equilibrated for 2 ns, followed by 8 ns of data collection. Additionally, a simulation of 512 molecules of octane was performed using the G45a3MOD force field, for comparison with the available experimental X-ray scattering data.

Radial distribution functions (RDFs) were calculated using the g_rdf program from the GROMACS software suite. From the RDFs, the X-ray scattering factors were calculated as the Fourier transform of the total electronic structure factor $h_{\mathrm{T}}(r)$, where

$$h_{\mathrm{T}}(r) = \left(\sum_{i,j \geq i} f_i f_j \chi_i \chi_j g_{ij}(r) \right) - 1 \qquad (2)$$

and the sum is over all types of atoms (CH_3, CH_2, O, H). χ_i is the mole fraction of atom type i. The scattering factor, f_i, is assumed to be independent of the scattering angle and proportional to the number of electrons of atom type i, and $g_{ij}(r)$ is the radial distribution function of atom types i and j.

Molecules were assigned to molecular clusters on the basis of oxygen−oxygen distance. First, a molecule was selected and all molecules with their oxygens within 0.35 nm were considered part of the cluster. The procedure was then repeated recursively on each of these molecules until no more molecules with oxygens within 0.35 nm could be located. A new molecule that was not yet assigned to a cluster was selected, and the process was repeated. This procedure was repeated until all molecules had been assigned to a cluster.

(25) Debolt, S. E.; Kollman, P. A. *J. Am. Chem. Soc.* **1995**, *117*, 5316−5340.
(26) Best, S. A.; Merz, K. M. J.; Reynolds, C. H. *J. Phys. Chem. B* **1999**, *103*, 714−726.
(27) Lindahl, E.; Hess, B.; van der Spoel, D. *J. Mol. Model.* **2001**, *7*, 306−317.
(28) Berendsen, H. J. C.; van der Spoel, D.; van Drunen, R. *Comput. Phys. Commun.* **1995**, *91*, 43−56.
(29) Hockney, R. W.; Goel, S. P. J. *J. Comput. Chem.* **1974**, *14*, 148.
(30) Miyamoto, S.; Kollman, P. A. *J. Comput. Chem.* **1992**, *13*, 952−962.
(31) Hess, B.; Bekker, H.; Berendsen, H. J. C.; Fraaije, J. G. E. M. *J. Comput. Chem.* **1997**, *18*, 1463−1472.
(32) Darden, T.; York, D.; Pedersen, L. *J. Chem. Phys.* **1993**, *98*, 10089−10092.
(33) Essmann, U.; Perera, L.; Berkowitz, M. L.; Darden, T.; Lee, H.; Pedersen, L. G. *J. Chem. Phys.* **1995**, *103*, 8577−8592.
(34) Berendsen, H. J. C.; Postma, J. P. M.; DiNola, A.; Haak, J. R. *J. Chem. Phys.* **1984**, *52*, 1695−1697.
(35) Daura, X.; Mark, A. E.; Van Gunsteren, W. F. *J. Comput. Chem.* **1998**, *19*, 535−547.
(36) Schuler, L. D.; Daura, X.; Van Gunsteren, W. F. *J. Comput. Chem.* **2001**, *22*, 1205−1218.
(37) Jorgensen, W. L.; Maxwell, D. S.; TiradoRives, J. *J. Am. Chem. Soc.* **1996**, *118*, 11225−11236.
(38) Jorgensen, W. L.; Madura, J. D.; Swenson, C. J. *J. Am. Chem. Soc.* **1984**, *106*, 6638.
(39) Jorgensen, W. L. *J. Phys. Chem.* **1986**, *90*, 1276.
(40) Jorgensen, W. L. *J. Phys. Chem.* **1983**, *87*, 5304.
(41) Van Gunsteren, W. F.; Berendsen, H. J. C. *Mol. Phys.* **1988**, *61*, 173.
(42) Villa, A.; Mark, A. E. *J. Comput. Chem.* **2002**, *23*, 548−553.
(43) Berendsen, H. J. C.; Postma, J. P. M.; van Gunsteren, W. F.; Hermans, J. In *Intermolecular Forces*; Pullman, B., Ed.; Reidel: Dordrecht, The Netherlands, 1981; pp 331−342.

Table 1. Physical Properties of Neat Octanol Calculated Using Various Force Fields

force field	ΔH_{vap}[f,g] (kJ/mol)	density[f,g] (g/L)
G43a2[a]	73.0 ± 0.2 (+2.8%)	852.2 ± 0.4 (+3.1%)
G45a3[b]	67.3 ± 0.2 (−5.2%)	805.2 ± 0.4 (−2.6%)
G45a3MOD[c]	71.3 ± 0.2 (+0.9%)	807.6 ± 0.4 (−2.3%)
OPLS-AA[d]	69.8 ± 0.2 (−1.7%)	823.9 ± 0.4 (−0.3%)
OPLS-DK[e]	68.6 ± 0.4 (−3.4%)	816 ± 3 (−1.3%)
experimental	70.98	826.3

[a] GROMOS96 parameter set with modified dihedrals.[27,44] [b] G43a2 with modified parameters for CH_3 and CH_2 groups.[36] [c] G45a3 with modified charges. [d] OPLS all atom force field.[37] [e] Modified OPLS nonbonded parameters with Amber-bonded parameters. Results taken from ref 25. [f] Values in parentheses indicate percent deviation from experimental values. [g] Experimental values taken from ref 45.

The moment of inertia tensor, I, was calculated for each cluster from

$$I = \sum_i m_i \begin{bmatrix} y^2 + z^2 & -xy & -xz \\ -xy & x^2 + z^2 & -yz \\ -xz & -yz & x^2 + y^2 \end{bmatrix} \quad (3)$$

where the sum is over all atoms in the cluster and m_i is the mass of atom i. The radius of gyration, R_G, was calculated as $\sqrt{Tr(I)/m_{Total}}$. The moment of inertia tensor was diagonalized to yield the principal moments of inertia, $\lambda_1 \geq \lambda_2 \geq \lambda_3$.

The chemical potential was calculated using the cavity-bias particle insertion method.[13] For these calculations, a 5-ns simulation was performed on a preequilibrated box of 1728 SPC water molecules. Particle insertion calculations were performed on this water system and the last 5 ns of the 0.1648 and 0.2849 mole fraction water systems. Insertions were attempted every 1 ps on a 60 × 60 × 60 grid of points, for a total of 1.08×10^9 insertions per system. Any grid points that had atoms closer than 0.26 nm were discarded, as the interaction energy would be extremely unfavorable because of overlap. The interaction energy, ΔU, between the inserted water molecule and the rest of the system was evaluated using a 1.4-nm group-based cutoff for both the Lennard−Jones and electrostatic calculations. The excess chemical potential was evaluated from

$$\mu_{\text{excess}} = -RT \ln\left(\frac{1}{\langle V\rangle}\langle V e^{-\Delta U/RT}\rangle\right) - RT\left(\ln\frac{1}{\langle V\rangle}\langle V p_{\text{cavity}}\rangle\right) \quad (4)$$

where angle brackets denote ensemble averages, V is the system volume, and p_{cavity} is the fraction of grid points where the nearest atom was greater than 0.26 nm away.

The total chemical potential is the sum of the ideal and excess chemical potentials, where the ideal chemical potential is given by

$$\mu_{\text{ideal}} = -RT \ln\frac{\rho}{\rho_{\text{ref}}} - RT \ln \chi \quad (5)$$

where ρ is the number density of water molecules, ρ_{ref} is the number density of water in the reference state, and χ is the mole fraction of water in the system. The first term accounts for the difference in chemical potential due to system density, while the second term is due to the ideal entropy of mixing. For these calculations, the reference system was taken as pure water at the simulated density of 32.5 molecules/nm^3.

Results

The calculated heats of vaporization (eq 1) and densities of neat octanol obtained using the different force fields are presented in Table 1. The GROMOS96[35] force field produces a density that is too high, which is a known deficiency of this force field. We next examined a modified version[36] of the

Table 2. Partial Atomic Charges for the $-CH_2-O-H$ Headgroup

force field[a]	q_{oxygen}	q_{hydrogen}	q_{carbon}
G45a3	−0.548	0.398	0.150
G45a3MOD	−0.563	0.407	0.156
OPLS-AA	−0.683	0.418	0.265
OPLS-DK	−0.700	0.435	0.265

[a] Force field names are the same as those in Table 1.

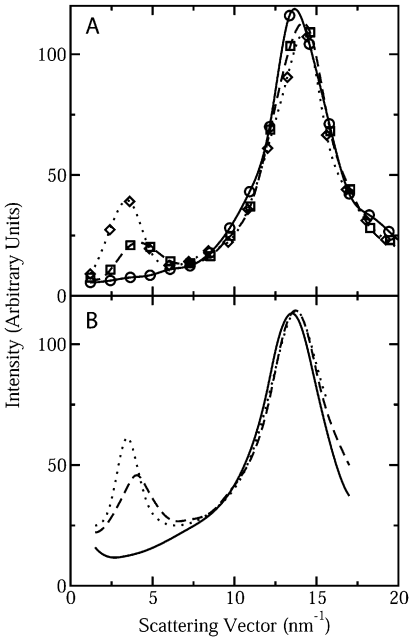

Figure 1. X-ray scattering intensities. (A) The calculated scattering intensities of octane (solid line with circles), neat octanol (dotted line with squares), and octanol with 0.259 mole fraction water (dashed line with diamonds) are shown. The lines represent a spline fit to the points obtained by Fourier transforming $h_T(r)$ (see eq 2). (B) Experimental data taken from ref 23.

GROMOS96 force field designated G45a3. This force field was designed to produce the correct density for long alkane chains but yields a density and heat of evaporation for octanol that are 5.2 and 2.6% too low, respectively. The corresponding errors for octane[35] are less than one percent. This indicates a problem with either the Lennard−Jones parameters of the hydroxyl oxygen or the partial charges used. From Table 2, it is obvious that the standard partial charges used in the GROMOS96 force field are lower than their counterparts in the OPLS family. Using the OPLS-UA charges with the GROMOS96 Lennard−Jones parameters yielded a heat of evaporation that was nearly twenty percent too high (data not shown). This prompted the scaling down of the OPLS charges until the heat of evaporation was in agreement with experimental results. This new parameter set designated G45a3MOD yielded the correct heat of vaporization but produced a density that was 2.3% too low. The results obtained with the OPLS all atom[37] force field and a slightly modified version of the OPLS united atom[25] force field are presented for comparison. As other work in our lab uses Gromacs software with parameters based on GROMOS96, we chose to use G45a3MOD for the rest of the simulations.

Simulated X-ray scattering intensities were calculated using eq 2, and the results are shown in Figure 1. The scattering of octane consists of a broad peak centered around 14 nm^{-1}. The addition of hydroxyl groups to give octanol results in a slight shift in position and intensity of this peak. However, most of

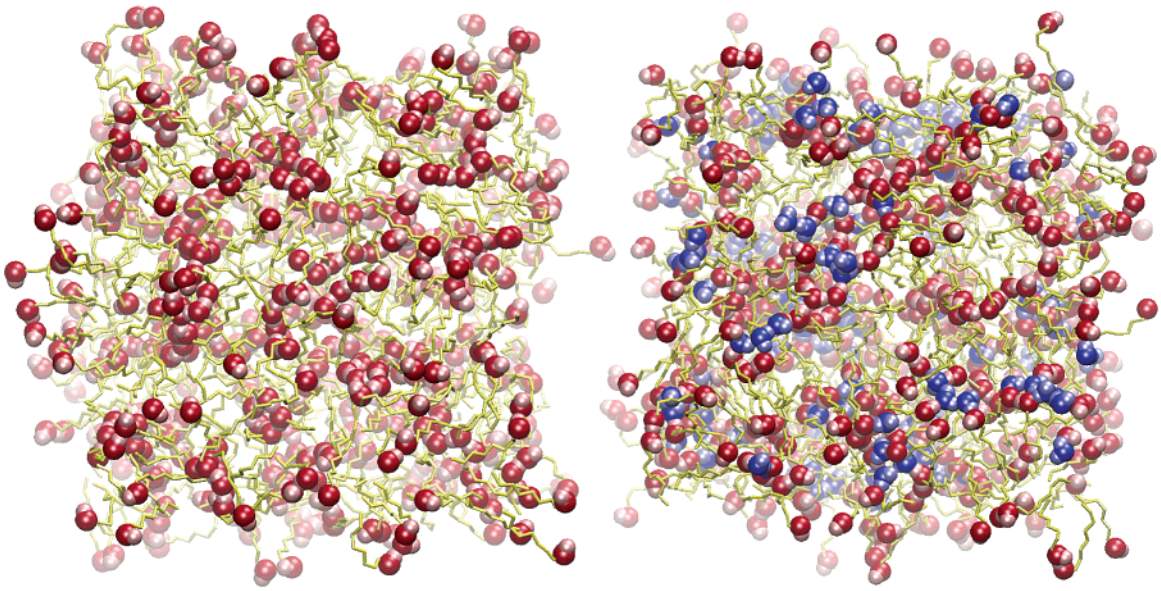

Figure 2. Sample snapshots of neat (left) and fully hydrated (0.259 mole fraction − right) octanol. Octanol is drawn as yellow lines for hydrocarbon chains, red spheres for oxygen, and pink spheres for hydrogen. Water is represented as dark blue spheres for oxygen and light blue spheres for hydrogen. Depth cueing is applied so atoms further away from the camera appear paler. All molecular graphics were created using VMD.[46]

the change results from the appearance of a new peak at ∼3.5 nm^{-1}. The addition of saturating (0.259 mole fraction) water results in a further increase in intensity of this peak and a shift to a slightly lower wavenumber.

Snapshots of the neat and fully hydrated systems are shown in Figure 2, while sample snapshots of individual clusters from neat, partially hydrated, and water-saturated octanol are shown in Figure 3. One obvious feature is the formation of hydrogen-bonded chains. The chains tend to be long and thin in neat octanol and become much longer and more spherical with increasing water content. In neat octanol, the hydrocarbon tails are oriented roughly perpendicular to the axis formed by the chain. In the water-saturated system, the clusters are more spherical with the hydrocarbon tails lying roughly on the surface of the sphere. There are a wide variety of structures present in both systems, including rings as well as both linear and branched chains. In both systems, it is clear that there are regions that are polar regions enriched in hydroxyl groups and nonpolar regions enriched in hydrocarbon tails. These polar regions surrounded by hydrocarbon tails have led to the use of the term "inverted micelle" when describing this system.[25,26]

The chainlike structure of neat octanol is evident in the plots of the oxygen−oxygen and oxygen−hydrogen (g_{O-O} and g_{O-H}, respectively) radial distribution functions (RDFs) shown in Figure 4. The peak at 0.18 nm in g_{O-H} is the hydrogen being donated to this molecule as part of a hydrogen bond. The peak at 0.28 nm represents the two neighboring oxygen atoms, one that donated the hydrogen from the previous peak and one that is accepting the hydrogen from the current molecule. The magnitude of the RDFs decays quickly because of the imperfect structure of liquids, but close examination of g_{O-O} reveals three peaks. At around 0.5 nm, the RDFs decay below 1.0, indicating the presence of hydrocarbon-enriched regions. At about 1.3 nm (see Figure 5), g_{O-O} rises above 1.0 again, indicating neighboring polar-enriched regions. This degree of long-range ordering is not found in simple liquids such as water and is due to the inhomogeneous distribution of atoms in this system.

Figure 5 displays g_{O-O} for neat, partially hydrated (0.128 mole fraction water), and water-saturated (0.259 mole fraction) octanol. The radius at which g_{O-O} decays below 1.0 increases with increasing water content, indicating that the radius of the polar-enriched regions is increasing. This is further verified by examining the width of the far polar-enriched region (inset Figure 5). The later quantity, when divided by two, is a good measure of the spherically averaged radius of the polar core of a hydrogen-bonded cluster. The distance between clusters can be estimated by measuring the distance between the point where the near polar enrichment ends and the far polar enrichment begins. If one-half of this quantity is added to the radius of the polar core, we arrive at an estimate of the total radius of a cluster.

RDFs are used to analyze a structure that is averaged over all cluster structures and all orientations over time. Thus, the shape will always be spherical. Alternatively, the moment of inertia tensor (eq 3) can be calculated, and from it, the radius of gyration and the ratios of the largest two principal moments of inertia to the smallest can be obtained. These are calculated individually for each cluster and then averaged over all clusters. The radius of gyration and ratios of principal moments of inertia, along with the estimates of the radius of the polar core and entire cluster from calculated RDFs, are given in Table 3. From the radii obtained, both from the RDFs and the radius of gyration calculations, it is clear that both the radius of the polar core and the total radius of the cluster increase upon the addition of water. The radius of gyration calculation leads to polar and total radii that are larger than the results from the RDFs, especially in the water-saturated system. The ratios of the moments of inertia give information about the shape of an object. A sphere will have equal principal moments, while a long, thin cylinder will have two moments that are much larger than the third. It is clear from the ratios of the principal moments of inertia that the clusters formed are not spherical. The polar cores tend to form prolate ellipsoids, with one dimension of the cluster longer than the other two, which are roughly equal. With increasing

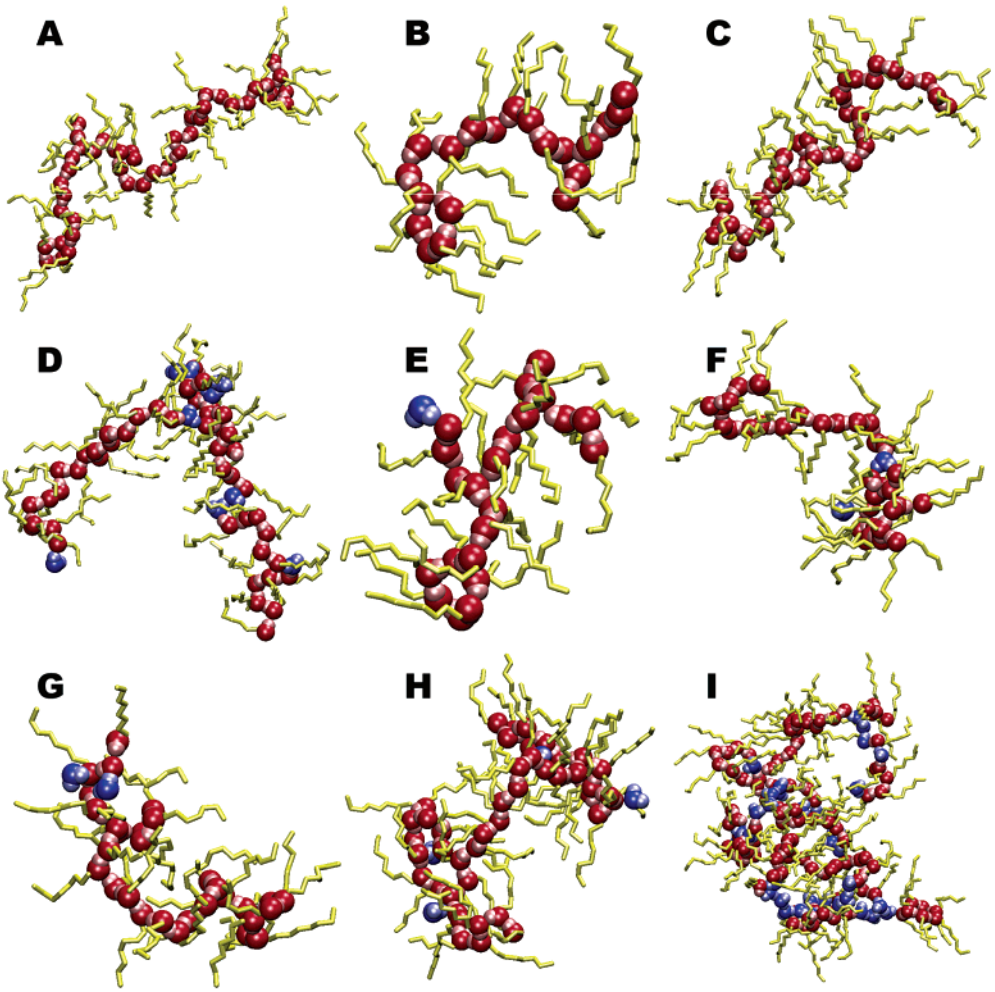

Figure 3. Sample snapshots of hydrogen-bonded clusters. Parts A−C are from neat octanol, D−F are from octanol with 0.128 mole fraction water, and G−I are from water-saturated (0.259 mole fraction) octanol. Octanol is represented as yellow lines for carbon chains, red spheres for oxygens, and pink spheres for hydrogens. Water is represented as dark blue spheres for oxygen and light blue spheres for hydrogen.

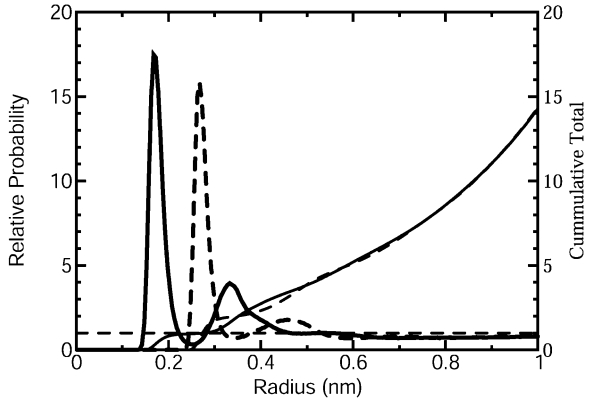

Figure 4. Radial distribution functions of neat octanol. g_{O-H} (thick solid lines) and g_{O-O} (thick dashed lines) are shown. The thin lines represent cumulative totals obtained by integrating over volume and multiplying by bulk density.

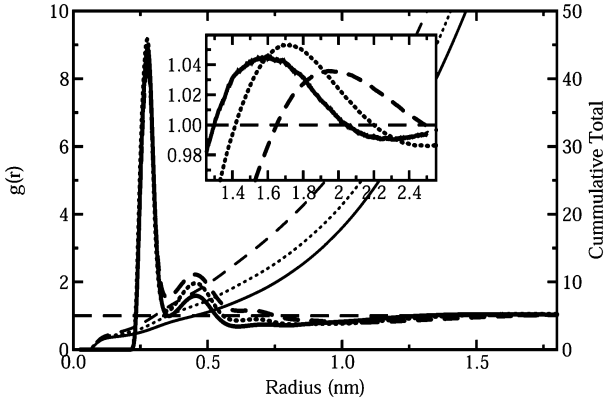

Figure 5. Radial distribution functions of hydrated octanol. The oxygen−oxygen radial distribution functions for neat (solid line), 0.128 mole fraction water (partially hydrated − dotted line), and 0.259 mole fraction water (saturated − dashed line) octanol are shown. The thin lines are cumulative totals obtained by integrating over volume and multiplying by bulk density. The inset shows the region from 1.3 to 2.5 nm, where the distribution functions rise above 1.0 again.

water content, the polar cores tend to become larger and more spherical, as indicated by an increase in R_G and a decrease in λ_1/λ_3 and λ_2/λ_3. Surprisingly, although the overall size of the cluster increases with increasing water content, the overall shape of the cluster stays virtually constant with changing water concentration, forming a prolate ellipsoid.

Clusters may be further characterized by the number of molecules that they are composed of. Figure 6 shows the distribution of cluster sizes in the three systems. In all three cases, there is a relative absence of two and three membered

Table 3. Measurements of Cluster Size

quantity[a]	neat	0.16 mole fraction water	0.259 mole fraction water
$\langle R_G$-polar$\rangle$[b] (nm)	0.46	0.60	0.69
$\langle R_G$-total$\rangle$[b] (nm)	0.79	0.91	1.00
R_{RDF}-polar[c] (nm)	0.38	0.39	0.42
R_{RDF}-total[d] (nm)	0.77	0.82	0.87
$R_{exp't}$-polar[e] (nm)	0.44		0.50
$R_{exp't}$-total[e] (nm)	0.72		0.86
$\langle\lambda 1/\lambda 3$ polar$\rangle$	1.98	1.84	1.81
$\langle\lambda 2/\lambda 3$ polar$\rangle$	1.79	1.65	1.63
$\langle\lambda 1/\lambda 3$ total$\rangle$	1.44	1.44	1.44
$\langle\lambda 2/\lambda 3$ total$\rangle$	1.31	1.32	1.32
$\langle N\rangle$[f]	7.48	16.68	28.40

[a] Polar indicates measurements including only oxygen atoms of clusters. Total indicates measurements including all oxygen atoms plus carbon chains. [b] Values from radius of gyration calculations. [c] Obtained by measuring the width of the far enriched peak of g_{O-O}; see Figure 5 inset. [d] Obtained by measuring the distance between the end of the near oxygen enrichment and the start of the far oxygen enrichment of g_{O-O}; see Figure 5. [e] From ref 24. [f] Average number of molecules per cluster.

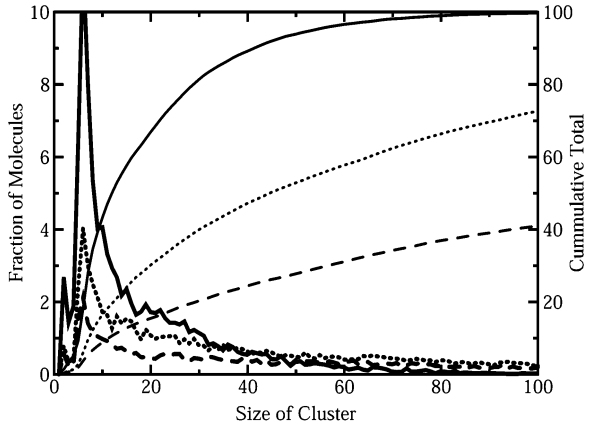

Figure 6. Cluster size distribution. The distribution of cluster sizes in neat (solid line), 0.128 mole fraction water (dotted), and 0.256 mole fraction water (dashed) octanol are shown. The thin lines represent cumulative totals obtained by integrating the thick lines.

clusters, and a large fraction of the molecules is contained in clusters of four to seven molecules. The distribution becomes flatter with increasing water content, shifting molecules from smaller clusters into larger ones. This shift is also evident in the average number of molecules per cluster (Table 3), which is nearly 4 times as high in water-saturated octanol as in neat octanol. The distributions of the hydrated systems still show a relative deficit of two and three membered clusters and an enrichment of clusters containing four to seven molecules, although it is not as pronounced.

For comparison with available infrared data, the fraction of "free" hydroxyl groups was calculated for neat octanol and found to be 5.5%. A free hydroxyl group was defined as one that did not donate its hydrogen as part of a hydrogen bond, and a hydrogen bond was defined as two oxygen atoms less than 0.35 nm apart and with an O−H−O angle of $<60°$.

The chemical potential of water was calculated (eqs 4 and 5) for pure water and two different concentrations of water in octanol. The results are shown in Figure 7 as a function of the number of insertions. The calculations yield chemical potentials of -26.6 ± 0.9 kJ/mol for pure water, -26.7 ± 0.2 kJ/mol for water in octanol with a 0.16 mole fraction, and -25.3 ± 0.5 kJ/mol for water in octanol with a 0.28 mole fraction water. When two phases in physical contact are at equilibrium, the

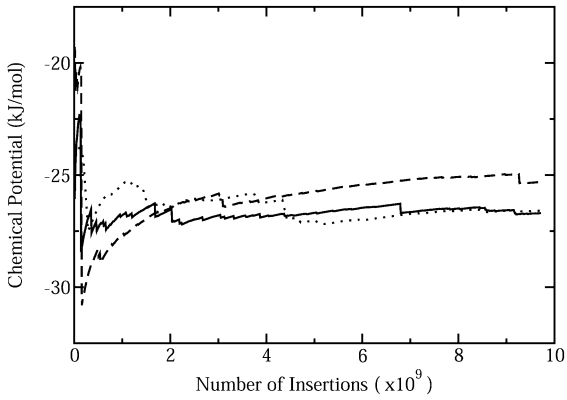

Figure 7. Convergence of chemical potential calculation. The chemical potential of water in octanol with 0.16 mole fraction water (solid line), octanol with 0.28 mole fraction water (dashed line), and pure water (dotted line) is shown as a function of the number of insertions.

chemical potential of each species must be the same in both phases. Thus, the equilibrium concentration of water in octanol will be the one that yields the same chemical potential as that of pure water. It appears that the calculated solubility of water in octanol is too low. The chemical potential does not change drastically with changing water content, which when coupled with the estimated errors makes it difficult to determine the exact saturation point. If we arbitrarily assume that the chemical potential is linear with mole fraction water, we obtain a saturation point of around 0.17, although there is a large uncertainty in the exact value. Using eq 6, we obtain a free energy for transferring water from pure water to saturated octanol of +9.35 kJ/mol.

$$\Delta G = -RT \ln \frac{[H_2O]_{oct}}{55.5\ M} \tag{6}$$

Discussion

The correlation time for the turnover of hydrogen-bonded clusters has been calculated previously by computer simulations[25] at 40 °C and found to be ~150 ps. Our simulations were performed at 25 °C, and so, the correlation time is expected to be somewhat longer. Even if the correlation time is much longer, it appears that our simulations are at least an order of magnitude longer than the lifetime of an individual cluster and, thus, we consider the analysis of cluster behavior to be well converged.

The X-ray scattering intensities calculated from these simulations (Figure 1) are in good agreement with the available experimental data. In one study by Vahvaselka et al.[23] on neat octanol, the scattering pattern was found to consist of a large principal maximum at ~13 nm^{-1} and a smaller side maximum at ~4 nm^{-1}. In another study[24] by Franks, Abraham, and Lieb (FAL), the scattering patterns of octane, neat octanol, and water-saturated octanol were obtained (Figure 1B). The scattering of octane consists of a single peak at about 13.5 nm^{-1}. Octanol displays the same main peak in addition to a smaller peak at about 4 nm^{-1}. The secondary peak increases in intensity and shifts to a slightly lower wavenumber with the addition of water.

When working with X-ray scattering from liquids, one cannot proceed from the scattering pattern to a model as one would with crystal diffraction. Instead, one must work "backwards",

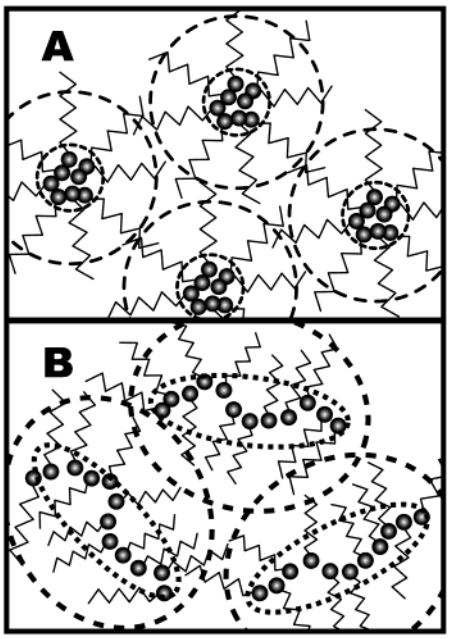

Figure 8. Schematic diagram of models of neat octanol. The model of Franks, Abraham, and Lieb[23] (A) is composed of hard spheres with a spherical polar core at the center. In our model (B), the clusters are prolate and are able to overlap slightly because of interdigitation of the carbon chains and other packing effects. The polar cores are more aspherical than the overall cluster and are formed primarily of rings of four to seven molecules and longer, more linear chains.

starting with a plausible model and tuning its parameters until the calculated scattering pattern matches the experimentally obtained one. There is no guarantee that the model obtained in this manner is correct, and it is possible that several models will yield the correct scattering pattern. Vahvaselka et al.[23] attempted to determine intermolecular oxygen−oxygen distances and coordination numbers. They obtained results for methanol, ethanol, propanol, and butanol, but their fitting procedure was unable to yield stable results for octanol. This indicates that the molecular organization of octanol may be different than that for shorter alcohols. FAL also performed X-ray scattering measurements and analyzed their data[24] in terms of a Percus−Yevick hard spheres model.[47] A rough sketch of their model is presented in Figure 8A. The model consists of polar cores with a radius $R_{exp't}$-polar that cannot approach each other closer than the total radius $R_{exp't}$-total.

Several measurements of cluster size are presented in Table 3. The values obtained from the simulated RDFs and the hard spheres model of FAL are in reasonable agreement. The radius of the polar core obtained from the RDFs was smaller than that of the hard spheres model, while the total radius was slightly larger. The differences are all less than the van der Waals radius of an oxygen atom, which is about 0.105 nm. The results from the radius of gyration calculations differ from the hard spheres model much more. This is to be expected because of the different types of averaging involved. From all three measurements, it is clear that both the average radius of the polar core and the average radius of the entire cluster increase with the addition of water.

From the radius of gyration calculations, it is evident that the clusters formed are not spherical (Table 3). The polar cores form prolate ellipsoids that become larger and more spherical with increasing water content. This may be explained by considering water's small size and enhanced hydrogen-bonding capacity relative to those of octanol. Water's small size allows it to fit into "tight" spaces that would be inaccessible to octanol, while its hydrogen-bonding capacity allows for more branching (see Figure 3I for example). It is unclear why the shape of the entire cluster, including hydrocarbon chain, should stay constant at different water concentrations while the shape of the polar core is changing. A partial explanation can be provided by looking at Figure 3. In neat octanol, the hydrogen-bonded chains have a roughly cylindrical shape with the carbon chains around the radius of the cylinder. Thus, the hydrocarbon chains will make the cluster more spherical. At high hydration, the clusters are more spherical, with the hydrocarbon tails around the perimeter. The addition of the hydrocarbon tails has much less of an effect on the shape than it did in neat octanol. This explains why the difference in shape is less drastic in saturated octanol than neat octanol, but it does not explain why the shape of the entire cluster remains essentially constant.

Using infrared spectroscopy, Grunwald and Pan[48] determined the concentration of hydroxyl groups that did not donate their hydrogen to a hydrogen bond. The value of 5.5% calculated from simulation is higher than the experimentally determined value of 3.8%. The free energy for donating a hydrogen can be calculated using

$$\Delta G = -RT \ln \frac{100 - \mathrm{ND}}{\mathrm{ND}} \qquad (7)$$

where ND is the percentage of nondonor hydrogens. The experimental value corresponds to a free energy of −8.0 kJ/mol, while the simulation yields a value of −7.1 kJ/mol, a difference of +0.9 kJ/mol. Thus, it appears that the simulation underestimates the free energy of hydrogen bonding by about 10%. The average cluster sizes (Table 3) and cluster size distribution (Figure 6) also points to an underestimation of hydrogen-bonding strength. Previous simulations by Debolt and Kollman[25] (DK) using a modified version of the OPLS-UA force field yield an average cluster size of 10.4 at 40 °C. Since their simulations were carried out at a higher temperature, we would expect that the average cluster size would be lower because of increased thermal fluctuations. However, the average cluster length obtained by DK is larger than the value 7.5 obtained from our simulations. The cluster size distribution obtained from our simulation is qualitatively very similar to the one obtained by DK. The distribution they obtained also displays a relative deficit of two and three membered clusters and an enrichment of four to seven membered clusters. The distribution obtained here is somewhat skewed toward smaller clusters compared to theirs, which is again consistent with hydrogen bonds that are too weak.

Our model of neat octanol is presented in Figure 8B. The liquid is composed of polymeric hydrogen bond networks of

(44) Van Gunsteren, W. F.; Billeter, S. R.; Eising, A. A.; Hunenberger, P. H.; Kruger, P.; Mark, A. E.; Scott, W. R. P.; Tironi, I. G. *Biomolecular Simulation: The GROMOS96 manual and user guide*; Hochschulverlag AG and ETH Zurich: Zurich, Switzerland, 1996.
(45) *CRC handbook of chemistry and physics*, 82 ed.; CRC Press: Cleveland, OH, 1994.
(46) Humphrey, W.; Dalke, A.; Schulten, K. *J. Mol. Graphics* **1996**, *14*, 33−38.
(47) Barker, J. A.; Henderson, D. *Rev. Mod. Phys.* **1976**, *48*, 587−671.
(48) Grunwald, E.; Pan, K.-C.; Effio, A. *J. Phys. Chem.* **1976**, *80*, 2937−2940.

varying lengths, with clusters of four to seven molecules being most common. DK calculated the fraction of clusters that form cyclic structures and found that almost all four, five, and six membered clusters form rings. As the clusters become larger, the fraction containing rings drops off. On average, each cluster has a radius of 0.79 nm, with a polar core of 0.46 nm. Overall, each cluster forms a slightly prolate ellipsoid, with a more aspherical polar core. The total radius of the cluster does not represent the distance of closest approach as it does in the model of FAL. It is possible for the total radius to overlap with neighboring clusters because of interdigitation of the side chains and other packing effects. The system can also be described in terms of spherical volumes that are enriched in hydroxyl groups. These regions have an average radius of 0.38 nm and are separated by about 0.78 nm. Our model, derived from realistic detailed simulations, is consistent with earlier computer simulations[25,26] and the interpretation of spectroscopic experiments.[48−51]

The model changes slightly with the addition of water. The clusters become larger, both in terms of the number of molecules involved and in radius. The average number of molecules per cluster nearly quadruples at saturating water concentration. This is in contrast to the model of FAL, where the number of molecules per aggregate went from 12 in neat octanol to 14 in hydrated octanol. We find that the shape of hydrogen-bonded clusters changes with hydration level. The polar cores become more spherical, which we attribute to water's ability to pack into small spaces and increased branching due to water's increased hydrogen-bonding capacity relative to that of octanol. The change in structure we observe is somewhat consistent with the model of FAL, where they do not find evidence for dramatic structural change upon hydration. Rather, we observe a subtler shift in the shape of molecular clusters, while the overall organization of the liquid remains relatively unchanged. This is consistent with earlier computer simulations[25,26] that show the formation of roughly spherical "inverted micelles" in water-saturated octanol.

The accuracy of our implementation of the cavity-bias particle insertion method can be evaluated by comparing the excess chemical potential we obtained for SPC water with previous calculations using different methods. Using thermodynamic integration with a group-based cutoff of 1.0 nm, Hermans et al.[52] obtained a value of −26.4 kJ/mol, while Mezei[53] obtained a value of −25.3 using the cavity-bias grand-canonical ensemble Monte Carlo. These values are in good agreement with the value −26.6 kJ/mol we obtained using the cavity-bias particle insertion method.

The results of the free energy calculations indicate that the solubility of water in octanol is too low (Figure 7). The free energy of transferring a water molecule from pure water to water-saturated octanol can be calculated using eq 6. The calculated saturation point leads to a free energy of 9.4 kJ/mol. This differs from the experimental value[54] 7.71 kJ/mol by +1.7 kJ/mol. A value of 11.3 was calculated[54] for the OPLS united atom model with TIP4P[55] water using the Gibbs ensemble Monte Carlo method. One reason for the better agreement of the solubility of water in octanol with a G45a3MOD force field compared to OPLS-UA may be the difference in hydrocarbon parameters. A comparison of the hydration free energy of butane reveals that OPLS-UA yields a value that is about 70% too high compared to experimental results. Thus, OPLS-UA hydrocarbons are not soluble enough in water, and water is likely too insoluble in the hydrocarbon phase. The hydration free energy of butane obtained using G45a3 is equal to the experimental result within the precision of the simulations. The OPLS-UA hydration free energies also show a trend of increasing deviation from experimental results with increasing chain length, so the error in the hydration free energy of octane may be larger. In contrast, the hydration free energy for octane using the G45a3 model is too high only by about 0.9 kJ/mol or 7%. The lower partial charges of the G45a3MOD model are consistent with the low hydrogen bond strength and the low solubility of water in octanol. It has been suggested[54] that the lack of polarizability of any of these force fields is also a factor. In particular, both SPC and TIP4P have been optimized for bulk water. The conditions in a water/octanol mixture are clearly different from bulk water, and this may influence the results.

There is considerable room for improvement of the G45a3MOD model. The density and fraction of nondonor hydrogens are both underestimated. The hydrocarbon parameters of G45a3 agree very well with experimental results, which points to possible improvements in the Lennard−Jones parameters of the hydroxyl oxygen and the partial charges used. The partial charge on oxygen is more than 20% higher in both of the OPLS-based force fields. The partial charge on oxygen is also more than 20% higher in a recent parametrization of methanol[56] on the basis of the GROMOS96 force field. A more thorough parametrization is needed to improve the agreement of the G45a3MOD model with experimental results. In particular, we believe that the partial charges need to be increased and the Lennard−Jones parameters of the hydroxyl oxygen need to be changed to reproduce the correct density and heat of evaporation with the modified charges. Additionally, the fraction of nondonor hydrogen bonds and the chemical potential of water provide further criteria for verification of the parameters.

Conclusions

We have used computer simulations to determine how the structures of octanol/water mixtures change upon addition of water. With increasing water concentration, hydrogen-bonded clusters of headgroups and water molecules become increasingly spherical. At different hydration levels, the experimental X-ray scattering factors are reproduced, so that the simulations provide an atomic-detail model of the underlying structure. Free energy calculations show that, for the GROMOS96-based force field, the solubility of SPC water in octanol is somewhat too low, which could be improved as part of a consistent reparametrization effort[42] by varying the octanol hydroxyl charges and/or the Lennard−Jones parameters for the interactions between water and the hydroxyl oxygen. The results from this work will be useful to further explore free energies of transfer of small

(49) Behrends, R.; Kaatze, U. *J. Phys. Chem. A* **2001**, *105*, 5829−5835.
(50) Paolantoni, M.; Sassi, P.; Morresi, A.; Cataliotti, R. S. *Mol. Phys.* **2001**, *99*, 1493−1502.
(51) Petong, P.; Pottel, R.; Kaatze, U. *J. Phys. Chem. A* **1999**, *103*, 6114−6121.
(52) Hermans, J.; Pathiaseril, A.; Anderson, A. *J. Am. Chem. Soc.* **1988**, *110*, 5982−5986.
(53) Mezei, M. *Mol. Phys.* **1987**, *61*, 565−582.
(54) Chen, B.; Siepmann, J. I. *J. Am. Chem. Soc.* **2000**, *122*, 6464−6467.
(55) Jorgensen, W. L.; Chandrasekhar, J.; Madura, J. D.; Impey, R. W.; Klein, M. L. *J. Chem. Phys.* **1983**, *79*, 926−935.
(56) Walser, R.; Mark, A. E.; Van Gunsteren, W. F. *J. Chem. Phys.* **2000**, *112*, 10450−10459.

molecules and peptides[21] and to improve the accuracy of simulations of lipids and membrane proteins.

Acknowledgment. D.P.T. is a Scholar of the Alberta Heritage Foundation for Medical Research. This work was supported by a grant from the National Science and Engineering Research Council of Canada. The authors wish to thank S. J. Marrink for insightful discussion and for the cluster analysis code. The authors would also like to thank N. P. Franks for providing the experimental data in Figure 1B.

JA027422O